Journal of ELECTRONIC MATERIALS, Vol. 44, No. 7, 2015
DOI: 10.1007/s11664-015-3671-2

Effects of Gd-Substitutions on the Microstructure, Electrical and Electromagnetic Behavior of M-Type Hexagonal Ferrites

ISHTIAQ AHMAD,[1,4] MAHMOOD AHMAD,[1] IHSAN ALI,[1] M. KANWAL,[1] M. S. AWAN,[3] GHULAM MUSTAFA,[1] and MUKHTAR AHMAD[2,5]

1.—Department of Physics, Bahauddin Zakariya University, Multan 60800, Pakistan. 2.—Department of Physics, COMSATS Institute of Information Technology, Islamabad 44000, Pakistan. 3.—ISIT, Sector H-11/4, Islamabad 44000, Pakistan. 4.—e-mail: drishtiaq_ahmad@yahoo.com. 5.—e-mail: ahmadmr25@yahoo.com

A series of Gd-substituted Ba-Co-based (M-type) hexaferrites having the chemical compositions of $Ba_{0.5}Co_{0.5}Gd_xFe_{12-x}O_{19}$ (x = 0.0, 0.2, 0.4, 0.6, 0.8, 1.0) were prepared by co-precipitation method. The pellets formed by co-precipitated powder were calcined at a temperature of 1200°C for 20 h. Final sintering was done at 1320°C for 4 h. From the x-ray diffraction analysis, it was revealed that all the samples showed M-type hexagonal structure as a major phase. The scanning electron microscope was used to examine the morphology of the sintered ferrites. The average grain size estimated by the line intercept method was found to be in the range of 2.8–1.0 μm. The room temperature DC resistivity increases with increasing Gd-contents to make these ferrites useful for high frequency applications and microwave devices. Lower values of coercivity (H_c) and higher saturation magnetization (M_s) may be suitable to enhance the permeability of these ferrites, which is favorable for impedance matching in microwave absorption. In addition, reflection coefficients for a sample was also measured from a frequency of 1 MHz to 3 GHz and a reflection peak was observed at about 2.2 GHz.

Key words: M-type hexagonal ferrites, Gd-substitution, SEM analysis, DC resistivity, M–H loops

INTRODUCTION

Barium-based hexagonal ferrites are being extensively used in industry as well as in domestic appliances. These materials can also be utilized in bulk form in many electrical and electronic devices, microwave devices, small motors, and, more recently, for magnetic recording media[1,2] due to their excellent magnetic and electrical properties. The magnetic properties of hexaferrites, such as their high saturation magnetization, corrosion resistivity, large magnetocrystalline anisotropy and high coercive field,[3] and their low cost of production have drawn considerable attention to these ferrites. In order to satisfy the utilization requirements of these compounds in many applications such as recording media, permanent magnets, microwave devices and magneto-optics, etc.,[4] many studies have been carried out to tailor the magnetic properties of hexaferrites. This can be accomplished by substituting Fe^{3+} ions with divalent and trivalent ions [such as rare earth (RE) ions] and tetravalent cations or combination of cations.[5,6] The Fe^{3+} ions in M-type hexaferrite structures are distributed on five different crystallographic sites, three octahedral (2a, 12k and $4f_2$), one tetrahedral ($4f_1$) and one trigonal bipyramidal (2b). In the magnetically ordered state in Ba hexaferrites, the 12k, 2a and 2b sites have their spins aligned parallel to each other in the crystallographic c-axis, but the $4f_2$ and $4f_1$ sites point in the opposite direction. The magnetic properties of the substituted hexaferrites strongly depend on the electronic configuration of the substituted cations. It is known that more electronegative ions have a preference to occupy

(Received June 9, 2014; accepted January 27, 2015; published online March 6, 2015)

octahedral co-ordination.[7,8] The saturation magnetization and other properties are related to the distribution of the substituted ions on these five crystallographic sites.[8] The substitution of cations at the Fe or Ba sites is an effective method to modify the physical, magnetic and electrical properties of barium hexaferrites. Generally, the barium hexaferrites are magnetic semiconductors, but divalent or tetravalent cations substituted at iron site may partially replace Fe^{3+} ions to increase their resistivity.[9] An improvement in the intrinsic magnetic properties of hexaferrites can be achieved by using the optimization of synthesis parameters and partial substitution for Ba or Fe sites or both. Many reports have recently shown that RE substituted M-hexaferrites have exhibited improved magnetic properties.[10,11] The improvement is largely associated with the increase of magnetocrystalline anisotropy, coercive force and magnetization as observed in La-doped strontium hexaferrites.[12] It has been reported[11,13] that the substitution of Sm ions can yield fine M-type ferrite powders resulting an increase in coercive field. Usually, the RE ions were substituted for Sr (Ba) or Fe, taking into accounts the ionic radii of the substituted elements.[10] Rare earth elements can also be used to inhibit the grain growth mechanism at high temperatures.[10] Rezlescu et al.[14] reported the RE substituted strontium ferrite nanoferrites with higher values of RE ions concentration (x = 0.2, 0.5, 1). It was observed from the results that an increased heat treatment was favorable to form single phase hexaferrites and to eliminate the intermediate phases that can deteriorate the magnetic properties of hexagonal ferrites. For many years, these ferrites have been extensively studied by many researchers using various synthesis techniques to produce different grain sizes and hence their effects on the magnetic and electrical properties.

The aim of the present work was to synthesize Gd-substituted Ba-Co-based M-type hexagonal ferrites and to study their structural, magnetic and electrical properties which are not reported frequently in the literature. Also, the lack of knowledge about the Gd-substituted M-type ferrites motivated us to synthesize and investigate these hexaferrites. Furthermore, rare earth (Gd) substitution was employed to inhibit the grains growth and to promote the fertilization reaction. It has also been reported that the lanthanides can be used to improve the mechanical materials hardness.[14]

EXPERIMENTAL

Samples Preparation

A co-precipitation method was employed to synthesize the Ba-Co-based hexaferrites with chemical composition ($Ba_{0.5}Co_{0.5}Gd_xFe_{12-x}O_{19}$, where x = 0.0, 0.2, 0.4, 0.6, 0.8, 1.0). The starting materials, i.e. barium acetate ($Ba(CH_3COO)_2$), iron chloride ($FeCl_3{\cdot}6H_2O$), cobalt acetate ($Co(CH_3COO)_2{\cdot}4H_2O$), gadolinium oxide ($Gd_2O_3$), sodium chloride (NaOH) and sodium carbonate (Na_2CO_3) of analytical grade having 99.9% purity were supplied by Merck (Germany) and de-ionized water was used to make the precursors. Required weights of salts of different metals for various compositions were mixed in 25 mL of distilled water according to stoichiometric calculations and stirred continuously with the help of a magnetic stirrer until a homogeneous solution was obtained. The precipitating agent was prepared by mixing NaOH and Na_2CO_3 in 100 mL of de-ionized water. The weights of NaOH and Na_2CO_3 for each sample were 1.40 g and 3.73 g, respectively, to ensure a pH value higher than 10, required for the chemical reaction to take place. When the precipitation completed, the solution was then thoroughly washed with de-ionized water several times. Addition of $AgNO_3$ confirmed the removal of NaCl by the precipitation technique because the solution was not milky. The solution was then filtered and dried in an electric oven at a temperature of 100°C for 24 h and ground. Using a Paul-Otto Weber hydraulic press, the powders were then pressed at ~35 kN for about 2 min to form the required pellets. These pellets were calcined at a temperature of 1200°C for 20 h and final sintering was done at 1320°C for 4 h.

Experimental Techniques

In order to confirm the phase purity of all the sintered samples, a JDX-3532 x-ray diffractometer at 40 kV and 30 mA equipped with Cu-kα (λ = 1.5406 Å with Ni filter) was used in the 2θ range from 15° to 75° at room temperature. A scanning electron microscope (SEM; Hitachi S4160) was used to examine the morphology and estimate the grain size of the sintered ferrites. The bulk density (d_B) for all the samples was measured by Archimedes principle using the following relationship[15]:

$$d_B = \left[\frac{W_{air}}{\text{Weightloss in the liquid}}\right] \times D_t \qquad (1)$$

where W_{air} represents the weight of the sample in air and D_t is the density of toluene, i.e. 0.857 g/cm^3. X-ray density (d_x) of all the ferrites was calculated using the relationship[15]:

$$d_x = \frac{2M}{N_A V} \qquad (2)$$

where M is the molecular weight of the sample, N_A is the Avogadro's number and V is the unit cell volume of hexagonal lattice.

The percentage porosity (%P) of all the samples was also calculated using the relationship[15]:

$$(\%)P = \left(1 - \frac{d_B}{d_x}\right) \times 100 \qquad (3)$$

DC resistivity (ρ) was measured by the two-probe method using a DC power supply model IP-2717

(Heath Kit) and a very sensitive electrometer model 610C (Keithly). In order to measure it, the following formula was used[15]:

$$\rho = \frac{RA}{t} \tag{4}$$

where R, A and t, are the resistance, area of cross-section and thickness of the pellet, respectively.

The temperature-dependent DC resistivity was also measured for all the samples in the temperature range of 40–150°C with steps of 10°C. Using the temperature-dependent resistivity data, the activation energies for all the ferrite samples were also calculated.

The magnetic parameters such as saturation magnetization (M_s), remanent magnetization (M_r) and coercivity (H_c) were measured by using a vibrating sample magnetometer (VSM; BHV-50; Riken Denish, Japan) at room temperature. The reflection coefficient (R_L) for a representative sample was measured at room temperature by an Agilent Impedance/Materials Analyzer (Model E4991A RF) over the frequency range of 1 MHz–3 GHz, with the 16453A test fixture.

RESULTS AND DISCUSSION

Phase Identification

The x-ray diffraction (XRD) patterns for all the samples of $Ba_{0.5}Co_{0.5}Gd_xFe_{12-x}O_{19}$ (x = 0.0, 0.2, 0.4, 0.6, 0.8, 1.0) are shown in Fig. 1. The observed peaks for all the samples were compared to those for standard patterns for M-type barium hexaferrite using the JCPDS card (00-043-0002). The analysis of observed patterns for all the samples shows that all peaks belong to the pure M-type hexagonal ferrite phase and no extra peak is observed, thereby confirming that all the samples are single phase without any impurity phase. The lattice parameters ('a' and 'c') were calculated using the following equation[16]

$$\mathrm{Sin}^2\theta = \frac{\lambda^2}{3a^2}(h^2 + hk + k^2) + \left(\frac{\lambda^2}{4c^2}\right)l^2 \tag{5}$$

Here λ represents the wavelength, a and c are the lattice parameters and hkl are the corresponding Miller indices.

The calculated values of the lattice parameters ('a' and 'c') as a function of x for all the samples are given in Table I. It can be observed that the values of 'a' and 'c' for all the samples are very close to the earlier reported values for M-type hexagonal structures.[17] From Table I, it can also be observed that the value of the lattice parameter 'a' remains almost unchanged in all Gd-substituted samples, while the value of the lattice parameter 'c' is decreasing with increasing Gd concentration. This behavior is similar to La-Co-substituted hexagonal ferrites, observed by Ogata et al.,[18] F. Kools et al.[19] and X. Liu et al.[12]

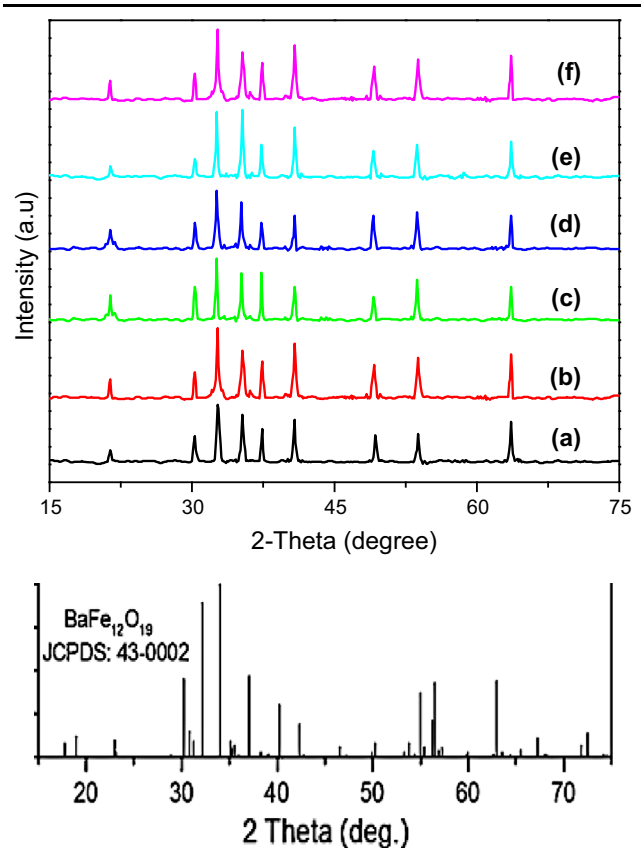

Fig. 1. XRD patterns of Gd-substituted M-type hexagonal ferrites $Ba_{0.5}Co_{0.5}Gd_xFe_{12-x}O_{19}$ (a) x = 0.0, (b) x = 0.2, (c) x = 0.4, (d) x = 0.6, (e) x = 0.8, and (f) x = 1.0.

Table I. Lattice parameters (a and c), c/a ratios, bulk density (d_B), x-ray density (d_x), porosity %(P) and grain size (D) for all hexagonal ferrites

Sample (x)	a(Å) ± 0.001	c(Å) ± 0.001	c/a ratios	d_B ± 0.01 (g/cm^3)	d_x (g/cm^3)	%(P)	D ± 0.02 (μm)
0.0	5.864	23.289	3.970	4.753	5.134	7.418	2.8
0.2	5.871	23.520	3.937	4.924	5.257	6.329	2.7
0.4	5.873	22.915	3.901	5.114	5.398	5.260	1.6
0.6	5.875	22.714	3.866	5.254	5.542	5.187	1.6
0.8	5.877	22.616	3.847	5.375	5.661	5.052	1.0
1.0	5.920	22.519	3.803	5.419	5.702	4.962	1.1

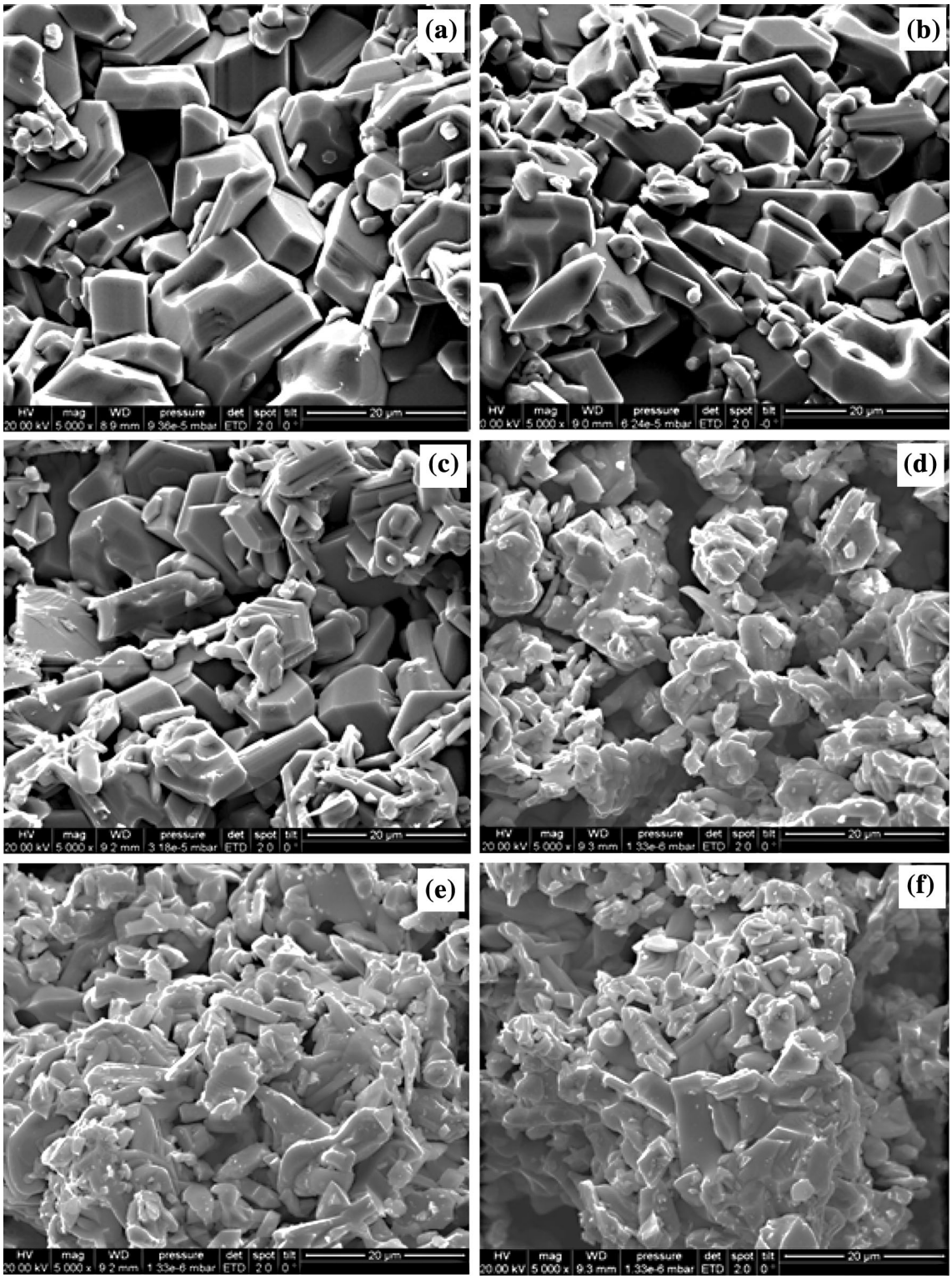

Fig. 2. SEM micrographs of Gd-substituted M-type hexagonal ferrites $Ba_{0.5}Co_{0.5}Gd_xFe_{12-x}O_{19}$ (a) $x = 0.0$, (b) $x = 0.2$, (c) $x = 0.4$, (d) $x = 0.6$, (e) $x = 0.8$, and (f) $x = 1.0$.

Microstructure and Grain Size

The SEM micrographs for all the samples of $Ba_{0.5}Co_{0.5}Gd_xFe_{12-x}O_{19}$ for various concentrations of Gd ($x = 0.0, 0.2, 0.4, 0.6, 0.8, 1.0$) are shown in Fig. 2. From these micrographs, the grain size was calculated using the line intercept method. The

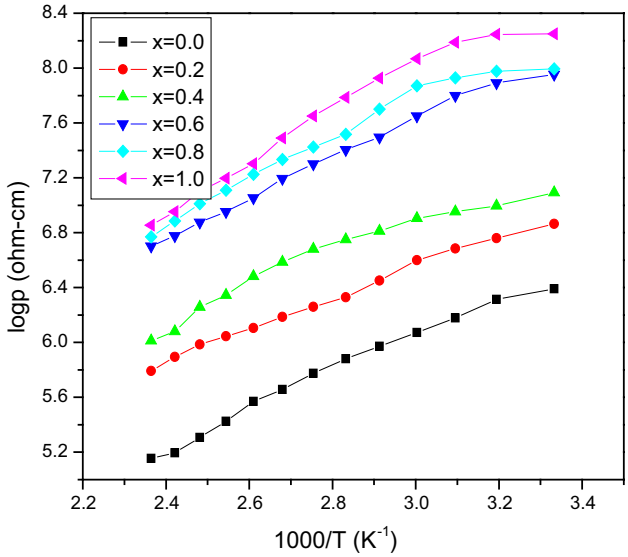

Fig. 3. Variation of resistivity as a function of temperature of M-type hexagonal ferrites $Ba_{0.5}Co_{0.5}Gd_xFe_{12-x}O_{19}$.

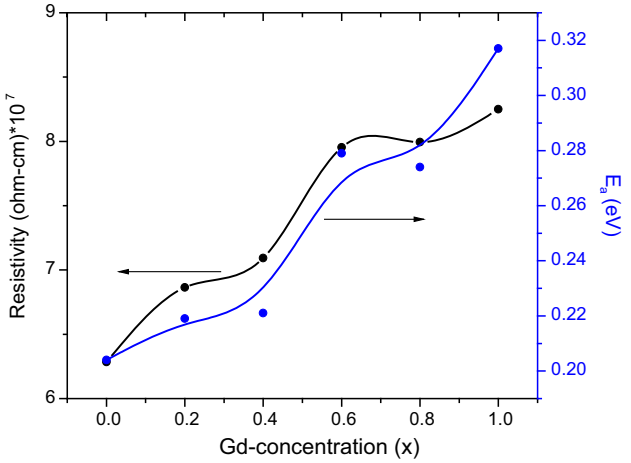

Fig. 4. Variation of resistivity and activation energy as a function of Gd-substitution for all M-type hexagonal ferrites.

average grain size estimated by this method as a function of Gd concentration is given in Table I. An average grain size (D) of about 2.8–1.0 μm can be estimated from the micrographs, which is quite large. Relatively higher sintering temperatures for longer times can be the reason for the larger average grain size achieved in these samples. Larger-sized grains are well known to enhance the microwave absorption in stealth technology.[20] This phenomenon can be better understood by keeping in view the fact that the ferrites with larger-sized grains are in more periodic arrangement due to the increased heat treatment, as in our case. When a magnetic field is applied to such type of materials, the spins can be easily aligned in the direction of the applied field due to this periodic arrangement. Consequently, high saturation magnetization can be observed in these materials which is favorable to enhance their permeability. Thus, enhanced permeability is suitable for impedance matching in microwave absorption or for the reduction of radar signatures in stealth technology.[21]

Furthermore, from these calculations, it was observed that the grain size was smaller for Gd^{3+}-substituted samples as compared to the pure one. This behavior of the grain size can be attributed to the replacement of RE ions by Fe ions as reported earlier by H. Taguchi et al., who stated that the presence of RE at Fe sites inhibits the grain growth.[22]

Physical Properties

The values of bulk density (d_B) calculated by Eq. 1 as a function of Gd contents (x) are provided in Table I, from which it can be seen that bulk density increases with increasing the Gd concentration (x) in the hexagonal lattice. This behavior may be attributed to the fact that the density of Gd (7.94 g/cm^3) is greater than that of Fe (7.874 g/cm^3).[23] As the Gd^{3+} is replacing the Fe^{3+} and due to larger charge concentration, the volume of the unit cell shrinks. Also, due to the smaller grain size, the surface contact area increases and hence the density increases. The values of x-ray density for all the samples as a function of Gd concentration (x) were calculated using Eq. 2 and are listed in Table I. The x-ray density increases from 5.134 g/cm^3 to 5.702 g/cm^3 with the increase in Gd contents (x). This increase can be explained on the basis of corresponding atomic weight of Gd (157.25 g), which is very high compared to that for Fe (55.85 g). Therefore, when Gd is substituted in the hexagonal lattice, the increase in atomic weight dominates the increase in unit cell volume, thus resulting in an increased value of x-ray density. A similar type of behavior was also observed by Ahmad et al. for RE-substituted W-type hexagonal ferrites.[15] The calculated values of d_x are in good agreement with the earlier reported value for this structure (5.3 g/cm^3).[24] Furthermore, it can also be observed that the values of bulk density are less than the x-ray density for all the samples, which can be attributed to the presence of pores in the material.[25] The values of porosity calculated by Eq. 3 for all the samples of $Ba_{0.5}Co_{0.5}Gd_xFe_{12-x}O_{19}$ (x = 0.0, 0.2, 0.4, 0.6, 0.8, and 1.0) as a function of x are listed in Table I. The porosity of the samples decreases with the Gd concentration x, which can be attributed to the increase in bulk density, smaller-sized gains and reduced unit cell volume as described earlier in the XRD analysis.

Electrical Measurements

Room temperature resistivity for all the samples was measured by the two-probe method using Eq. 4, and the calculated values as a function of

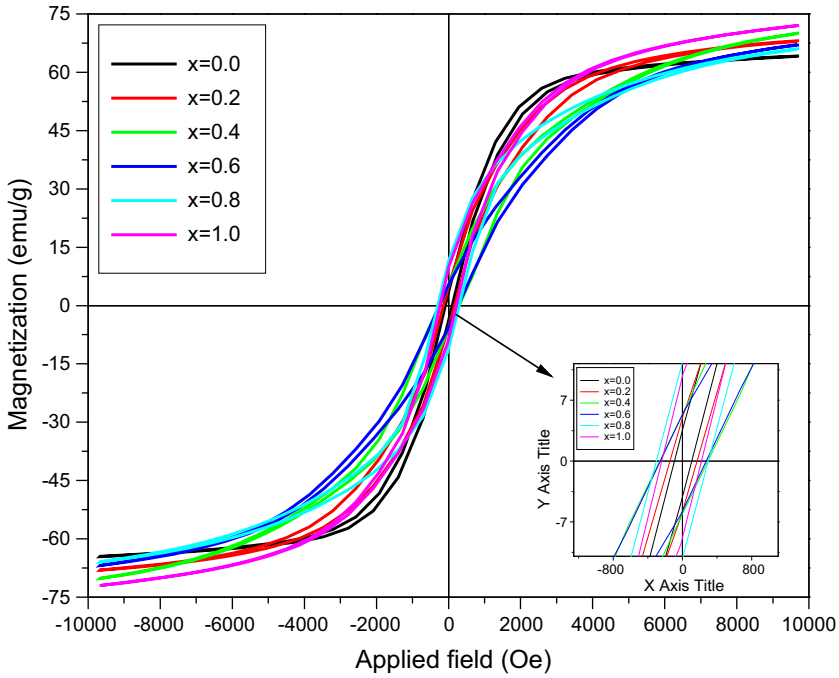

Fig. 5. M–H loops of Gd-substituted M-type hexagonal ferrites $Ba_{0.5}Co_{0.5}Gd_xFe_{12-x}O_{19}$.

Table II. Magnetic parameters as a function of Gd-substitution for all M-type hexagonal ferrites

Sample (x)	M_s (emu/g)	M_r (emu/g)	M_r/M_s	H_c (Oe)
0.0	64.33	3.55	0.06	100.15
0.2	68.09	4.96	0.07	147.94
0.4	70.05	5.38	0.08	271.67
0.6	67.02	5.33	0.08	256.33
0.8	66.03	11.44	0.17	302.50
1.0	72.01	9.79	0.14	242.19

Gd-concentration are shown in Fig. 3, from which it is clear that the resistivity increases from 6.285×10^7 Ω-cm to 8.250×10^7 Ω-cm with increasing Gd concentration in the hexagonal lattice, which may be explained as follows;

1. In the present work, since the samples are prepared by the wet method, a fine particle size is expected, which increases the grain boundary area resulting in an increased value of the resistivity. This effect has also been observed by Stijintjes et al.[26]
2. As the Gd concentration is increased, which has alarger value of resistivity (1.310×10^{-4} Ω-cm) as compared to that for Fe (1.0×10^{-5} Ω-cm), the room temperature resistivity of these ferrites increases.[27] Due to the increased values of resistivity with increasing Gd concentration, the present samples can be used for high-frequency applications and microwave devices where low eddy current losses are desirable.[28]

Temprature-dependent resistivity of all the samples was also measured in the temperature range of 300–450 K. The corresponding graphs of $1000/T$ versus log (ρ) for each sample are shown in Fig. 3, from which it can be seen that the behavior in each sample follows the Arrhenius equation;

$$\rho = \rho_o \exp(\Delta E/K_B T) \quad (6)$$

where ΔE is the activation energy, T is the absolute temperature, and K_B is Boltzmann's constant.

The decreasing trend of resistivity with increasing temperature in the present samples dictates that they exhibit a semiconducting behavior, which is the well-established fact for all the ferrites.[29] Using the temperature-dependent resistivity data, the activation energies were also calculated for all the samples. The activation energies calculated from the slope of the graphs ($1000/T$ vs. $\log\rho$) for all the samples are shown in Fig. 4, from which it can be observed that the value of the activation energy is increasing with the increase in Gd concentration (x) from 0.204 eV to 0.317 eV. This increase in activation energy seems to be due to the increase in

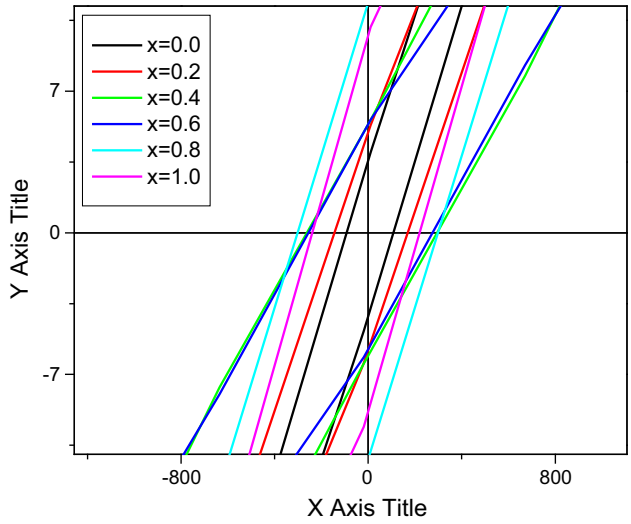

Fig. 6. Representation of low field coercivities of M-type hexagonal ferrites $Ba_{0.5}Co_{0.5}Gd_xFe_{12-x}O_{19}$.

resistivity with the increase in x. This behavior supports the established theory that a sample with high resistivity would have high activation energy and vice versa.

Magnetic Measurements

The M–H loops for all the sintered samples of the compound $Ba_{0.5}Co_{0.5}Gd_xFe_{12-x}O_{19}$ (x = 0, 0.2, 0.4, 0.6, 0.8, 1) are shown in Fig. 5. It can be seen that the coercive field H_c has a value of a few hundred oersteds which reveals that the prepared ferrites have soft characters due to higher calcination or sintering temperatures for longer durations. It has been reported in earlier published data that the coercivity of a few hundred oersteds is one of the necessary conditions for electromagnetic (EM) materials,[30,31] hence making these ferrites suitable for the suppression of electromagnetic interference (EMI). The values of the coercive field (H_c) with increasing Gd concentration is provided in Table II. It can be observed that Gd-substituted samples have larger values of H_c as compared to the unsubstituted one. This behavior of H_c may be due to the enhancement of the magneto-crystalline anisotropy[10,13] with anisotropic Fe^{2+} ions locating on 2a sites, as usually found in RE ions substitution.[10] In addition, we have achieved a lower value of coercivity (H_c) for the investigated samples as compared to the earlier reported values of hexagonal ferrites for the same structure. The lower value achieved makes these materials suitable for high-frequency applications, enhancement of permeability and for the suppression of EMI.[31]

The saturation magnetization (M_s), remanence (M_r) and squareness ratios (M_r/M_s) for all the samples were also obtained from the M–H loops and their values are provided in Table II. It can be observed that the values of saturation magnetization (M_s) were found to be in the ranges of (64.33–72.01 emu/g) which are quite large compared to the earlier reported values for M-type hexagonal ferrites prepared by other methods.[32] In addition, the values of M_r and M_r/M_s were found to be in the ranges of 3.55–11.44 emu/g and 0.06–0.17 emu/g, respectively, for all the samples. Furthermore, it has been observed that the substitution of Gd^{3+} ions for Fe^{3+} ions causes the higher values of magnetization in these ferrites. This is because Gd has a higher value of magnetic moment (7.94 μ_B) as compared to that for Fe (5 μ_B). The H_c in the present work is lower and M_s is higher than the values reported by Xiao-Hui Wang et al.[33] Figure 6 represents the low field coercivities of M-type $Ba_{0.5}Co_{0.5}Gd_xFe_{12-x}O_{19}$ (x = 0.0–1.0) hexagonal ferrites. The relationship between the permeability and saturation magnetization can be representated by the following equation[34]

$$\mu_i = 1 + \frac{(4\pi M_s)^2}{(4\pi M_s)H_a - (f/2.8)^2 + j\alpha(4\pi M_s)(f/2.8)} \quad (7)$$

where f is the frequency, M_s is the saturation magnetization and H_a is the magnetic anisotropy field. From the above equation, it is obvious that permeability increases with the increase of M_s and the decrease of H_a. Due to high M_s, low H_c and larger sized grains, these materials can be used to improve the permeability and absorption of microwaves. It is also known that the enhanced absorption bandwidth and the minimum reflection losses can be achieved by higher permeability of ferrites. Therefore, excellent electromagnetic properties can be achieved by microwave-absorbing materials filled with the investigated ferrites to be considered as potential candidates for microwave-absorbing purposes.

Microwave Absorption Properties

The frequency-dependent (1 MHz–3 GHz) reflection coefficient (Γ) for the M-type $Ba_{0.5}Co_{0.5}Gd_xFe_{12-x}O_{19}$ (x = 0.2) hexaferrite at room temperature is shown in Fig. 7. The reflection coefficient (Γ) is reduced with the rise of the applied field frequency. The absorption peak appeared at a specific frequency of 2.2 GHz. The peaking nature occurs due to resonance when the electrons jumping frequency between Fe^{3+} and Fe^{2+} becomes equal to the applied field frequency.[35,36] A similar kind of peak has also been observed in the case of the M-type Ba hexagonal ferrites.[37] A material with low reflection loss, wide absorption bandwidth and low matching thickness is useful for good microwave-absorber material. There exists no ideal material which satisfies all these requirements. The reflection coefficient in the present study decreased with the increase of the frequency of the applied AC field. Therefore, the synthesized materials may be beneficial for high-frequency applications such as

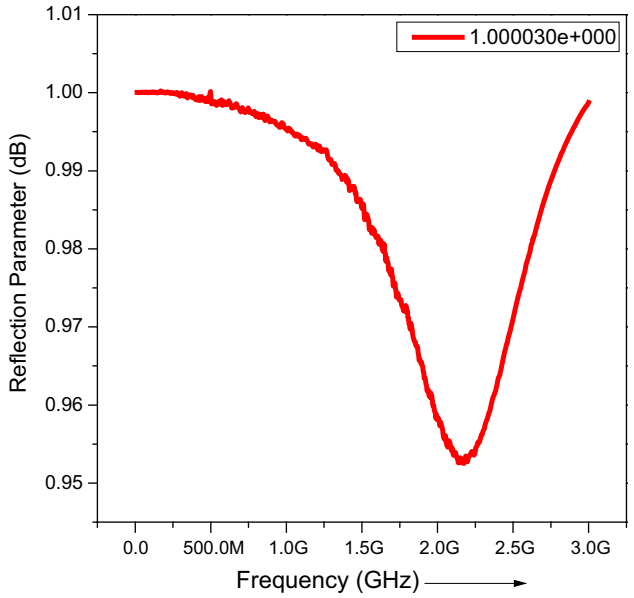

Fig. 7. Frequency-dependent (1 MHz–3 GHz) reflection coefficient (Γ) for M-type $Ba_{0.5}Co_{0.5}Gd_xFe_{12-x}O_{19}$ (x = 0.2) hexaferrite at room temperature.

microwave radiation absorption, camouflaging purposes, and the attenuation of EMI.

CONCLUSIONS

On the basis of the above results and discussion for Gd-substituted M-type hexagonal ferrites, the following conclusions can be drawn from this study:

1. Single phase M-type hexagonal ferrites can be successfully synthesized by the coprecipitation method by substituting Gd ions in place of Fe ions in the hexagonal lattice.
2. The average grain size was observed to be smaller for Gd-substituted hexagonal ferrites, which is due to the well-established fact that the replacement of RE by Fe inhibits the grain growth. In addition, larger-sized grains were achieved for all the samples, which is favorable for microwave absorption.
3. The value of room temperature DC resistivity was observed to increase with increasing Gd concentration for these hexagonal ferrites.
4. Temperature-dependent resistivity of all the samples shows a decreasing trend with increasing temperature, demonstrating the semiconducting nature of these ferrites.
5. The low value of H_c (of a few hundred oersteds) and higher saturation magnetization were achieved for all the samples, as compared to previous work.
6. Minimum reflection was observed at a frequency of about 2.2 GHz, showing that there is a maximum absorption at this frequency.

Because to all these different parameters, it can be affirmed that these ferrites may be potential candidates for high-frequency applications and for microwave-absorbing purposes.

ACKNOWLEDGEMENT

The authors gratefully acknowledge Prof. Dr. Shehzad Naseem, CSSP, University of the Punjab, Lahore for providing the necessary experimental facilities.

REFERENCES

1. H. Yamamoto, M. Nagakura, and H. Terada, *IEEE Trans. Magn.* 26, 1144 (1990).
2. G. Li, G.G. Hu, H.D. Zhou, X.J. Fan, and X.G. Li, *Mater. Chem. Phys.* 75, 101 (2002).
3. F. Kools, A. Morel, R. Grossinger, J.M. Le Breton, and P. Tenaud, *J. Magn. Magn. Mater.* 1270, 242 (2002).
4. H. Pfeiffer, R.W. Chantrell, P. Gornert, W. Schuppel, E. Sinn, and M. Rosler, *J. Magn. Magn. Mater.* 125, 373 (1993).
5. A. Ghasemi and A. Morisako, *J. Alloys Compd.* 456, 485 (2008).
6. X. Tang, Y. Yang, and K. Hu, *J. Alloys Compd.* 477, 322 (2009).
7. M.V. Rane, D. Bahadur, S.D. Kulkarni, and S.K. Date, *J. Magn. Magn. Mater.* 195, L256 (1999).
8. S. Ounnunkada and P. Winotai, *J. Magn. Magn. Mater.* 301, 292 (2006).
9. B. Kaur, M. Bhat, F. Licci, R. Kumar, K.K. Bamzai, and P.N. Kotru, *Mater. Chem. Phys.* 103, 255 (2007).
10. S. Ounnunkad, *Solid State Commun.* 138, 472 (2006).
11. J.F. Wang, C.B. Ponton, and I.R. Harris, *J. Magn. Magn. Mater.* 298, 122 (2006).
12. X. Liu, W. Zhong, S. Yang, Z. Yu, B. Gu, and Y. Du, *J. Magn. Magn. Mater.* 238, 207 (2002).
13. L. Lechevallier, J.M. Le Breton, J.F. Wang, and I.R. Harris, *J. Magn. Magn. Mater.* 269, 192 (2004).
14. N. Rezlescu, C. Doroftei, E. Rezlescu, and P.D. Popa, *J. Alloys Compd.* 451, 492 (2008).
15. M. Ahmad, F. Aen, M.U. Islam, S.B. Niazi, and M.U. Rana, *Ceram. Int.* 37, 3691 (2011).
16. B.D. Cullity, *Elements of X-ray Diffraction*, Vol. 338 (Upper Saddle River: Prentice Hall, 1977), p. 102.
17. G. Listsardakis, I. Manolakis, and K. Efthimiadis, *J. Alloys Compd.* 427, 194 (2007).
18. Y. Ogata, Y. Kubota, T. Takami, M. Tokunaga, and T. Shinohara, *IEEE Trans. Magn.* 35, 3334 (1999).
19. F. Kools, A. Morel, P. Tenaud, M. Reossignol, O. Isnard, R. Grossinger, J.M. Le Breton, and J. Teillet, *Proceeding of the International Conference on ferrites ICF8* (Kyoto Japan, 2000), p. 437.
20. A. Goldman, *Modern Ferrite Technology*, 2nd ed. (New York: Springer, 2006), p. 83.
21. M. Ahmad, R. Grössinger, M. Kriegisch, F. Kubel, and M.U. Rana, *Curr. App. Phys.* 12, 1413 (2012).
22. H. Taguchi, *J. Phys. IV Fr.* 7, c1-299 (1997).
23. C. Kittel, *Introduction to Solid State Physics*, 5th ed. (New York: John Wiley & Sons Inc., 1956), p. 24.
24. J. Smit and H.P. Wijin, *Ferrites* (London: Cleaver-Hume Press, 1959), p. 185.
25. S.A. Safaan and A.M. Abo, *J. Magn. Magn. Mater.* 302, 362 (2006).
26. T.G.W. Stijintjes, A. Broese Vas Groenou, R.F. Pearson, J.E. Knowles, and P. Rankin, *Proceedings of the International Conference* (1970).
27. M. Ajmal and A. Maqsood, *Mater. Sci. Eng. B* 139, 164 (2007).
28. M.J. Iqbal and R.A. Khan, *J. Alloys Compd.* 478, 847 (2009).
29. A.A. Sattar, H.M. El-sayed, K.M. El-shokrofy, and M.M. El-Tabey, *J. Appl. Sci.* 5, 162 (2005).
30. M. Ahmad, R. Grössinger, M. Kriegisch, F. Kubel, and M.U. Rana, *J. Magn. Magn. Mater.* 332, 137 (2013).
31. A. Globus, *J. Phys. (Paris) Colloq.*, 1, C1 (1977).

32. I. Ali, M.U. Islam, M.S. Awan, M. Ahmad, M.N. Ashiq, and S. Naseem, *J. Alloys Compd.* 550, 564 (2013).
33. X.-H. Wang, T.-L. Ren, L.-Y. Li, and L.-S. Zhang, *J. Magn. Magn. Mater.* 184, 95 (1998).
34. L.Z. Wu, J. Ding, H.B. Jiang, L.F. Chen, and C.K. Ong, *J. Magn. Magn. Mater.* 285, 33 (2005).
35. M.B. Reddy and P.V. Reddy, *Appl. Phys.* 24, 975 (1991).
36. S.C. Watawe, B.D. Sarwede, S.S. Bellad, B.D. Sutar, and B.K. Chougule, *J. Magn. Magn. Mater.* 214, 55 (2000).
37. G. Mu, N. Chen, X. Pan, H. Shen, and M. Gu, *Mater. Lett.* 62, 840 (2008).